Determination of the Exciton Binding Energy in Single-Walled Carbon Nanotubes

Zhenjia Wang,* Hermen Pedrosa, Todd Krauss, and Lewis Rothberg†

Department of Chemistry, University of Rochester, Rochester, New York 14627, USA

(Received 13 August 2005; published 3 February 2006)

We report that measurements of the Raman intensity versus applied voltage are sensitive to filling of the density of states and enable us to measure the second band gap in specific semiconducting single-walled carbon nanotubes (SWNTs). Raman scattering preferentially selects sets of SWNTs whose excitonic transitions are resonant with the incident or scattered photon energies. Simultaneous measurement of the electronic gap and exciton resonance allows us to infer binding energies for the exciton of 0.49 ± 0.05 and 0.62 ± 0.05 eV for tubes of $(10, 3)$ and $(7, 5)$, respectively. Metallic SWNTs exhibit no excitonic feature.

DOI: 10.1103/PhysRevLett.96.047403 PACS numbers: 78.67.Ch, 71.20.Tx, 71.35.−y, 78.30.Na

Single-walled carbon nanotubes (SWNTs) are one-dimensional (1D) tubular graphitic macromolecules that are typically microns long and ~1 nanometer wide [1]. SWNT structures can be characterized by two integers, (n, m), that define both their diameter and chirality [2], and when $n - m$ is not divisible by 3, the nanotubes are semiconducting. The optical properties of carbon nanotubes are intrinsically important for potential applications in photonics [3] and also provide insight into their structural and electrical properties. The absorption and emission of semiconducting SWNTs are dominated by excitonic effects [4–9] but measurement of central features such as the exciton binding energies in semiconducting nanotubes remains elusive. The magnitude of the exciton binding energy relative to thermal energies is extremely important to the photophysical properties of semiconductors and has been a topic of active investigation and controversy in one-dimensional conjugated organic semiconductors for more than a decade [10,11]. Recent experiments on carbon nanotubes [12–15] support a picture where excitonic effects are important to the optical spectroscopy. Spectral congestion due to inhomogeneity of carbon nanotube samples, however, renders optical measurements of SWNT exciton binding energies difficult since the interband transition associated with free carrier generation is obscured by much stronger excitonic transitions from neighboring nanotubes. Wang *et al.* [12] have circumvented this difficulty with elegant two-photon fluorescence excitation spectroscopy experiments on SWNT where they observe Rydberg series of excitonic features and deduce binding energies of ~400 meV for the first excitonic band in semiconducting SWNTs.

In the present work, we measure the binding energy of the second band excitons in isolated SWNTs using resonant Raman scattering (RS) during electrochemical doping of SWNT. Subsets of SWNTs can be monitored individually by selecting SWNT with a particular radial breathing mode (RBM) frequency. For semiconducting SWNTs, the dominant intermediate electronic state in the RS matrix elements is excitonic in character and RS therefore selects nanotubes whose exciton absorption is resonant with the incident or scattered photon. At the same time, the excitonic absorption strength at the incident photon energy and, consequently, the intensity of RS for the phonon modes will be affected by electrochemical doping. Depletion of electrons from the valence band or addition of electrons to the conduction band will reduce the exciton binding energy and lead to broadening of the excitonic resonance due to screening of the interactions between the electron and hole [16]. Therefore, the behavior of the Raman intensity with applied bias allows us to track the density of states and measure the electronic band gap. We can make optical measurements that are sensitive to excitonic features and electrical ones that are sensitive to charge carrier energetics simultaneously. The combination enables a straightforward comparison of the band gap and exciton transition energy (i.e., laser photon energy) to determine the exciton binding energy. We find the binding energy for the exciton associated with the second allowed transition in isolated semiconducting SWNTs to be 0.49 ± 0.05 eV for carbon nanotubes with (n, m) of $(10, 3)$ and 0.62 ± 0.05 eV for those with (n, m) of $(7, 5)$, similar to those predicted theoretically [8] for SWNTs with similar radii. As expected, metallic nanotubes show no signs of excitonic behavior but our data provide evidence of band splittings due to trigonal warping.

Raman studies of electrochemically doped SWNT bundles or thin SWNT films have been carried out before [17–21] but the complex morphologies of the bundles do not allow facile penetration of electrolyte ions into the bundles. In addition, intertube interactions can also alter an individual nanotube's electronic behavior due to large contact areas [22]. These problems obscure the fine structure in the spectral features and can mask the true applied bias.

Individual SWNTs were isolated in surfactant micelles of sodium dodecyl sulfate (SDS) in D_2O using ultrasonic agitation and centrifugation [23]. The SWNTs were synthesized by the high pressure CO (HiPCO) reaction and purchased from Carbon Nanotechnologies, Inc. Our TEM images and narrow Raman mode linewidths confirm that

the SWNTs are isolated. A 40 μl drop of dilute solution containing SWNTs was deposited onto a clean indium tin oxide (ITO) coated glass slide that served as a working electrode. A single Pt electrode serving as both reference electrode and counterelectrode was used with an electrolyte solution of either 0.5*M* sodium sulfate or sodium chloride to vary the potential applied to the SWNTs. Previous work has documented that Pt forms an Ohmic contact to SWNT [24]. Thus the applied voltage is all dropped across the SWNT as we have implicitly assumed in equating the applied potential with the movement in the Fermi level. We observe the same dependence of resonance Raman spectra on electrochemical bias in both electrolyte solutions which also suggests good contact between the electrode and SWNT. Raman spectra from SWNTs on ITO were obtained using a confocal microscope with a 1.4 numerical aperture (NA) oil-immersion objective and 632.8 nm excitation [25]. Scattered light was collected with the same objective, passed through dichroic and holographic notch filters to block scattered excitation light, dispersed by a spectrometer, and measured with a liquid-nitrogen-cooled CCD camera. The spatial resolution is approximately 300 nm.

Figure 1(a) shows Raman spectra of SWNTs at one location on the substrate in the radial breathing mode (RBM) spectral region. The four Raman peaks at 196 cm^{-1}, 222 cm^{-1}, 254 cm^{-1}, and 282 cm^{-1} are a result of scattering from four sets of different diameter tubes whose optical transition energies are near resonant with the incident or scattered photon energy. The band intensities depended on voltage and were reversible under repeated cycling [Fig. 1(b)]. Assignment of specific indices (n, m) to the tubes with RBM modes at 254 cm^{-1} and 282 cm^{-1} is straightforward, following the work of Bachilo *et al.* [5]. These carbon nanotubes are semiconducting with indices (10, 3) and (7, 5), respectively. The incident photon energy (1.96 eV) is resonant with the exciton associated with the second valence to conduction band transition V_2-C_2 for (10, 3) and the scattered photon (1.93 eV) is resonant with the same transition for (7, 5). Possible resonances with V_1-C_2 and V_2-C_1 are ruled out on the basis of selection rules [26] while V_1-C_1 transitions are too low energy to be resonant with 632.8 nm excitation. The assignment of the indices for SWNT with RBM modes at 196 cm^{-1} and 222 cm^{-1} is less clear and will be discussed below but we can nevertheless infer that they are metallic. Using the relationship between RBM frequency ν and tube diameter d_t in nm, $\nu = 223.5/d_t + 12.5$ [5], those tube diameters would be 1.22 nm and 1.07 nm. From the empirical Kataura plot [27], we find that only metallic tubes of these diameters can be resonantly excited at 632.8 nm. We recorded SWNT Raman spectra on several samples and many areas of each sample and only the Stokes shifts evident in Fig. 1(b) were observed albeit with variable relative intensities.

Figure 2 presents the RS intensities of the RBM modes with applied voltage for the semiconducting SWNT tubes

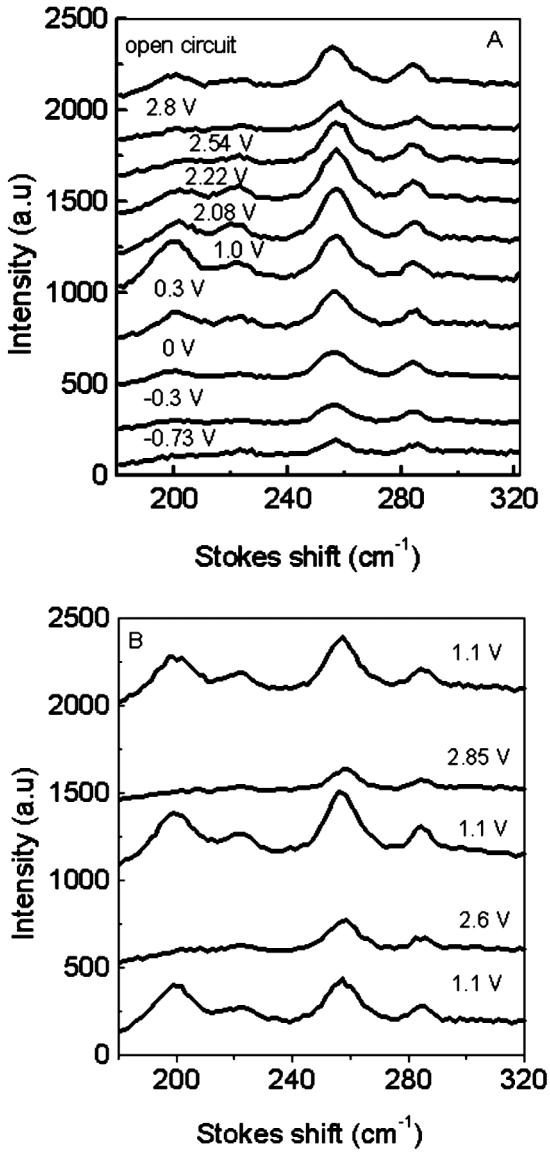

FIG. 1. (a) Raman spectra of the RBM modes of SWNTs vs applied potential. (b) Raman spectra as voltage are cycled illustrating reversible doping. The experimental sequence in time is from zero to positive voltage and then from zero negative voltage.

(254 cm^{-1} and 282 cm^{-1}). The data of Fig. 2 can be rationalized on the basis of electrochemical filling of the second valence and conduction bands. Low Raman intensity is observed when free charge carriers in the valence and conduction bands are available to quench excitons and broaden the associated resonance from which the RS derives intensity. Conversely, we observe high plateaus in Raman intensity over a range of 2.45 ± 0.05 V for the 252 cm^{-1} phonon mode and 2.55 ± 0.05 V for the 282 cm^{-1} mode as determined by looking at sharp changes in derivative at the plateau edges. These reflect the electronic band gap where the energy is sufficient to fully occupy the valence band but the second conduction band remains empty. Therefore, the exciton binding energy is

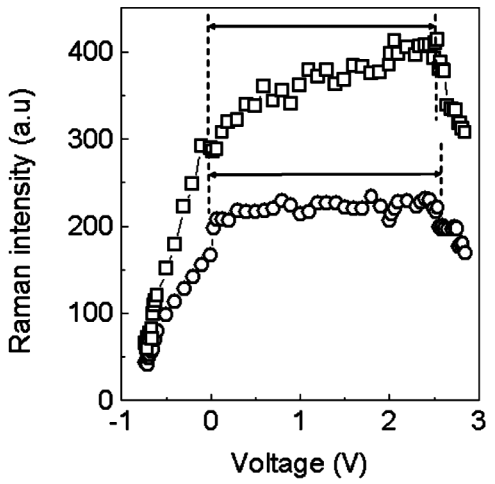

FIG. 2. Raman intensity of the RBM modes at 254 cm^{-1} (squares) and 282 cm^{-1} (circles) of semiconducting SWNTs vs applied potential. The arrows over the regions where the Raman intensity is flat with changes in applied bias represent the electronic band gaps of the nanotubes under study as described in the text.

the difference between the width of the Raman plateau and the incident (1.96 eV) or scattered photon (1.93 eV). The measured binding energies are then 0.49 ± 0.05 eV for (10, 3) (252 cm^{-1}) nanotubes and 0.62 ± 0.05 eV for (7, 5) (282 cm^{-1}) nanotubes. These binding energies are very close to the results of theoretical calculations of the binding energies of excitons associated with the E_{22} transitions for similar diameter tubes (7, 6) and (10, 0), 0.47 eV and 0.57 eV, respectively [8].

Similar data on Raman intensity versus applied potential can be obtained for the radial breathing modes assigned to metallic nanotubes as shown in Fig 3. In those cases, it is difficult to make definitive assignments for the indices (n, m) since many tubes of large diameter are near resonant with 1.96 eV incident photons. Indeed, Fig. 4 shows that the RBM frequencies appear to vary with applied potential suggesting an inhomogeneous distribution of SWNTs under study. In contrast, there is no variation in frequency for the RBM bands associated with semiconducting tubes or for the *D* and *G* bands. Figures 3(a) and 3(b) present the Raman intensity data versus applied potential and, like the semiconductor case, these can be understood based on filling of the density of states. We expect increases in intensity as the participating valence bands are populated [-0.8 eV to 0.7 eV in Figs. 3(a) and 3(b)] and diminution in intensity at large bias (> 2 eV) as filling of the conduction band reduces the density of available final states. We assume that excitons do not exist in the metallic SWNTs and that the RS is now resonantly enhanced by the interband transition V_1-C_1. Therefore, large Raman intensities will be observed for tubes whose peaks in the valence band and conduction band state densities are separated by approximately the laser photon energy. Naïvely, one would therefore expect a plateau in the intensity data of around

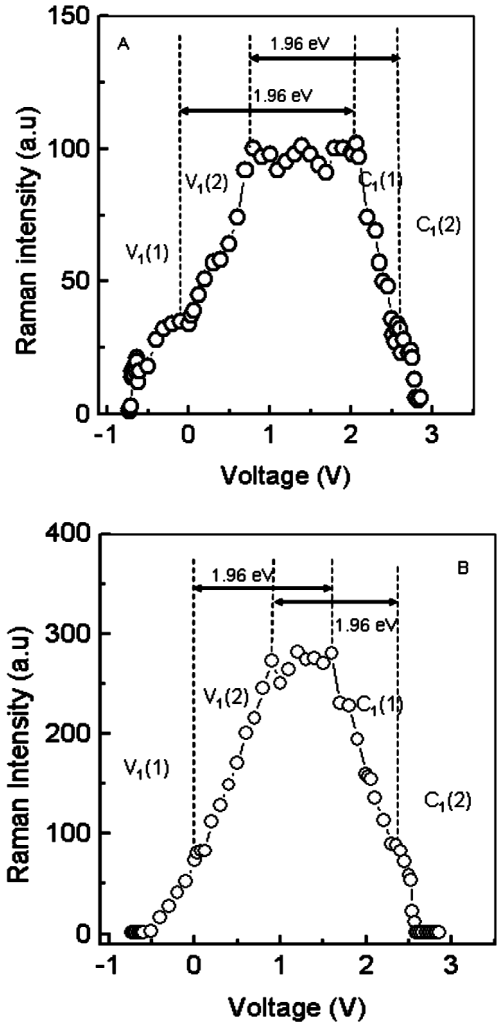

FIG. 3. Raman intensities of RBM modes of metallic tubes at (a) 222 cm^{-1} and (b) 196 cm^{-1} vs applied potential. The arrows represent interband transitions between density of states spikes that appear as kinks in the Raman intensity vs bias. Those are associated with bands $V_1(1)$, $V_1(2)$, $C_1(1)$, and $C_1(2)$ as labeled. Transitions are allowed between $V_1(1)$ and $C_1(1)$ or between $V_1(2)$ and $C_1(2)$ that are resonant with incident light at 1.96 eV.

1.96 eV rather than $\sim$1.4 eV and 1 eV as observed in Figs. 3(a) and 3(b), respectively. We believe this discrepancy results from trigonal warping which causes both V_1 and C_1 to be split into subbands $V_1(1)$ and $V_1(2)$ and $C_1(1)$ and $C_1(2)$. The optical transitions obey selection rules allowing only $V_1(1) \rightarrow C_1(1)$ and $V_1(2) \rightarrow C_1(2)$ and our experiment selects RS from SWNT where these transitions are at 1.96 eV. The width of the plateau therefore corresponds to the $V_1(2)$ to $C_1(1)$ separation as indicated schematically in the figures. Assuming symmetric splittings, and that we have correctly identified kinks on the figure reflecting the underlying DOS, it implies band splittings of $\sim$0.5–0.6 eV. These are somewhat larger than reported by STM studies [28] and it is possible that the kinks in our data are manifestations of lower valence and higher conduction bands.

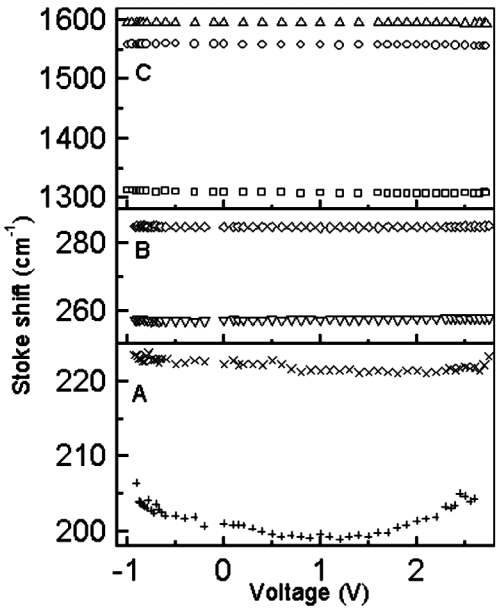

FIG. 4. Raman frequencies of the RBM modes, the *D* band, and the *G* band phonons vs applied potential. (a) and (b) show the RBM modes, (c) the *D* bands at 1310 cm^{-1}, and the *G* bands at 1557 cm^{-1} and 1595 cm^{-1}.

We have also studied the higher frequency Raman modes (*D* and *G* bands) of the carbon nanotubes and their behavior with applied potential. The *G* bands have two peaks at 1558 cm^{-1} and 1595 cm^{-1} corresponding to C-C stretching vibrations while the *D* band at 1310 cm^{-1} is well known to be associated with defects. Each of these bands possesses a potential dependence of the Raman intensity similar to that of the RBM modes except averaged over semiconducting and metallic band filling behaviors. The frequencies of the C-C stretching bands are independent of applied potential unlike that of corresponding modes in quasi-one-dimensional conjugated polymers [29], indicating that the stiffness of SWNTs results in large carrier delocalization and very small polaron binding energy (i.e., small lattice deformations) so that carriers in SWNTs can be expected to have very high mobility [30].

In conclusion, we use the applied bias dependence of RS intensity in semiconducting SWNT to measure the binding energy of second band excitons. Measurement of the exciton binding energy cannot be done by STM since excitons must be photogenerated. We obtain values of 0.49 eV for (10, 3) and to be 0.62 eV for (7, 5), close to those from the theoretical calculations of Zhao and Mazumdar that include electron-electron correlation [8]. The exciton binding energies are a critical parameter for optoelectronic applications and the ones we observe are large compared to thermal energies so that semiconducting carbon nanotubes can be expected to have photophysics more like conjugated polymers than direct gap inorganic semiconductors such as GaAs. Our data are consistent with no significant binding energy between electron and hole in metallic SWNTs and intraband splittings of ~0.5 eV due to trigonal warping in zigzag SWNT.

We thank NSF DMR-0309444, Research Corporation (R-10733), and the New York State Office of Science and Academic Research (C-020085) for funding.

Note added.—Additional work on the exciton binding energy in carbon nanotubes using two-photon excited photoluminescence was reported recently [31] and is in agreement with the work presented here.

*To whom correspondence should be addressed.
Email address: wangz@chem.rochester.edu
†Email address: rothberg@chem.rochester.edu

[1] S. Iijima, Nature (London) **354**, 56 (1991).
[2] R. Saito, G. Dresselhaus, and M. S. Dresselhaus, *Physical Properties of Carbon Nanotubes* (Imperial College Press, London, 1998).
[3] A. Hartschuh *et al.*, Science **301**, 1354 (2003).
[4] C. D. Spataru *et al.*, Phys. Rev. Lett. **92**, 077402 (2004).
[5] S. M. Bachilo *et al.*, Science **298**, 2361 (2002).
[6] O. J. Korovyanko *et al.*, Phys. Rev. Lett. **92**, 017403 (2004).
[7] V. Perebeinos *et al.*, Phys. Rev. Lett. **92**, 257402 (2004).
[8] H. Zhao and S. Mazumdar, Phys. Rev. Lett. **93**, 157402 (2004).
[9] C. L. Kane and E. J. Mele, Phys. Rev. Lett. **90**, 207401 (2003).
[10] E. M. Conwell, in *Organic Electronic Materials*, edited by R. Farchioni and G. Grosso (Springer-Verlag, Berlin, 2001), pp. 127–180.
[11] Y. Cao *et al.*, Nature (London) **397**, 414 (1999).
[12] F. Wang *et al.*, Science **308**, 838 (2005).
[13] Y. Z. Ma *et al.*, Phys. Rev. Lett. **94**, 157402 (2005).
[14] L. Huang and T. D. Krauss (to be published).
[15] M. Ichida *et al.*, Phys. Rev. B **65**, 241407(R) (2002).
[16] G. D. Mahan, Phys. Rev. **153**, 882 (1967).
[17] J. N. Barisci *et al.*, J. Electrochem. Soc. **150**, E409 (2003).
[18] G. U. Sumanasekera *et al.*, J. Phys. Chem. B **103**, 4292 (1999).
[19] P. Corio *et al.*, Chem. Phys. Lett. **370**, 675 (2003).
[20] L. Kavan *et al.*, J. Phys. Chem. B **105**, 10 764 (2001).
[21] M. E. Itkis *et al.*, Nano Lett. **2**, 155 (2002).
[22] M. Stoll *et al.*, Chem. Phys. Lett. **375**, 625 (2003).
[23] M. J. O'Connell *et al.*, Science **297**, 593 (2002).
[24] S. J. Tans *et al.*, Nature (London) **386**, 474 (1997).
[25] Z. Wang *et al.*, Proc. Natl. Acad. Sci. U.S.A. **100**, 8638 (2003).
[26] A. Gruneis *et al.*, Phys. Rev. B **67**, 165402 (2003).
[27] R. B. Weisman, Nano Lett. **3**, 1235 (2003).
[28] M. Ouyang *et al.*, Science **292**, 702 (2001).
[29] M. Baitoul *et al.*, Phys. Rev. B **68**, 195203 (2003).
[30] P. L. McEuen and J. Y. Park, MRS Bull. **29**, 272 (2004).
[31] J. Maultzsch *et al.*, Phys. Rev. B **72**, 241402(R) (2005).